19th Australasian Fluid Mechanics Conference
Melbourne, Australia
8-11 December 2014

Sheared Turbulent Convection of a Buoyant Fluid from a Horizontal Porous Plate

M. P. Kirkpatrick[1], N. Williamson[1], S. H. Starner[1] and S. W. Armfield[1]

[1]School of Aerospace, Mechanical and Mechatronic Engineering
The University of Sydney, Sydney, New South Wales 2006, Australia

Abstract

Experimental results are presented for a turbulent boundary layer in which buoyant surface convection is created using fresh and salt water. The experiments were performed in an open channel laboratory flume, with a surface buoyancy flux generated using a uniformly distributed up-flow of fresh water through the porous lower surface of the flume into the denser salt water flow above. Measurements were taken with a simultaneous planar Particle Image Velocimetry / Laser Induced Fluorescence system. We quantify the effect of the surface mass, momentum and buoyancy fluxes on the structure of the boundary layer and discuss the usefulness of this experimental model for representing thermal convective boundary layers.

Introduction

Turbulent boundary layers with buoyant surface convection occur in a wide variety of environmental contexts including the Earth's atmosphere, oceans, rivers, lakes, reservoirs and estuaries, as well as engineering applications such as air-conditioning and natural ventilation of building spaces, food processing, and power generation. In the majority of these situations buoyant convection results from a temperature differential between a solid surface and the fluid.

While thermal convective boundary layers can be studied using point-type experimental measurement techniques such as hot and cold-wire anemometry, they are less amenable to the application of laser diagnostic techniques such as Particle Image Velocimetry (PIV) and Laser Induced Fluorescence (LIF). Two of the major difficulties posed are: the optical distortions due to variations in refractive index of the fluid resulting from the variations in temperature; and the low intensity resolution obtainable in thermal LIF measurements.

Both of these issues can be overcome in experiments which use fresh and salt water rather than temperature to generate the buoyancy differences. Refractive index matching can be achieved by adding ethanol to the fresh water stream, while the addition of dye to only one of the streams gives high intensity resolution LIF measurements of the density field.

In this paper we investigate the possibility of modelling a turbulent convective boundary layer using salt and fresh water. Results from three data sets are presented: a turbulent boundary layer with no surface flow, with a non-buoyant surface flow, and with a positively buoyant surface flow.

Method

Figure 1 shows the experimental set-up. A neutrally-stable, turbulent open-channel flow of saline water is generated in the development section of a 250 mm wide by 5 m long laboratory water flume. For the experiments presented here the height of the flow δ_b was in the range $35-43.5$ mm. The neutral flow develops over a distance of 3m, corresponding to $70-80\delta_b$. The fully developed turbulent boundary layer then enters a 1.5m section of the flume in which the base consists of a series of six 250×250 mm plenums, each covered by a 1.5mm thick perforated stainless steel plate. The plates have holes of diameter $D_j = 1.5$mm, with open/closed area ratio of $A_r = 21\%$. In order to provide a hydraulically smooth surface, the plates are overlaid with a fine wire mesh with diameter 50 μm and pitch 80 μm. This system allows a uniformly distributed influx of water through the surface into the over-flowing boundary layer.

The simultaneous PIV/PLIF system uses a dual cavity 532 nm Nd:YAG pulsed laser (Quantel Evergreen) capable of pulse energies up to 145 mJ. Images are recorded using two 2048×2048 pixel monochrome, double-shutter CCD cameras (PCO.2000). Full details of the rig and PIV/PLIF system are given in [1]. The main difference in our current set up is a new prismatic periscope, designed and built in-house, that sits within the flume downstream of the measurement zone and reflects the laser sheet so that it passes through the measurement zone parallel to the base of the flume. With this system we were able to maintain effective illumination down to the surface without generating unwanted reflections or glare from the plate and mesh.

Measurements were taken using the PIV/LIF system to obtain simultaneous time-series of the velocity and buoyancy fields in a 45 mm measurement zone located at the downstream end of the convection section. With the current camera set-up, this measurement zone corresponds to approximately 900×900 pixels on the cameras, giving a LIF pixel resolution of 0.05 mm. The PIV fields were processed down to an interrogation area resolution of 16×16 pixels and grid step resolution of 6 pixels, corresponding to a spatial resolution of 0.8×0.8 mm and 0.3 mm, respectively. At this level of resolution the subpix failure rate was approximately 0.25%, and the median-test rejection rate was in the range $2.8-3\%$.

This set-up enabled us to obtain velocity measurements down to a distance of 0.45 mm above the surface, and LIF measurements to a distance of 0.1 mm from the surface, which correspond to $y^+\approx5$ and 1 respectively. Thus we have been able to obtain measurements down to the top of the laminar sublayer for the velocity field and to well within the laminar sublayer for the density field. There is scope for obtaining higher resolution in the future by matching the measurement zone more closely to the field of view of the cameras and by optimizing the data acquisition and PIV processing parameters.

In each run images were recorded at a frequency of 2 Hz over a 2 minute period, with a time difference $\Delta t = 5$ ms between the image pairs. Fluorescence for the LIF imaging was achieved using Rhodamine 6G dye added to the fresh surface flow water tank with a concentration of 40 ppb. For the PIV imaging, 10–100 μm spherical glass beads at a concentration of 12.5 g/m^3 were used as tracer particles. Ethanol was added to the fresh water to match the refractive indices between the fresh and salt water.

Processing of the PIV and LIF images was done using a set of Matlab scripts that we have developed over the course of this project. The PIV processing is built around PIVSuite developed by Jiri Vejrazka. The PIV and LIF fields are matched by first mapping their coordinate arrays from pixel to world co-

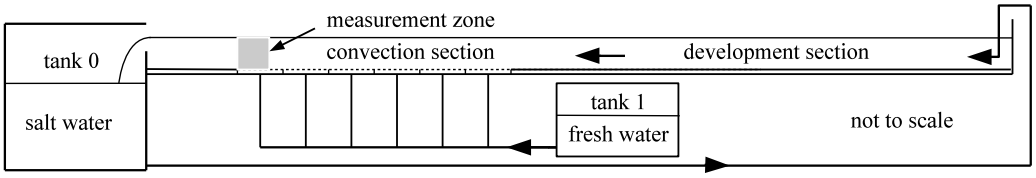

Figure 1: Schematic of experimental set-up.

ordinates using 3rd order polynomial mapping matrices generated by processing images of a 5×5 mm checkerboard target placed in the measurement zone. The LIF and PIV fields are then matched by binning the LIF at 6×6 pixels to match the PIV grid resolution and then interpolating both onto a regular 0.3×0.3 mm Cartesian grid. We also generate a full resolution unbinned LIF field on a 0.05×0.05 mm grid.

The raw LIF images are normalized as,

$$I(x,y,t) = (I_r(x,y,t) - \bar{I}_{bg})/(\bar{I}_c(x,y,t) - \bar{I}_{bg}), \qquad (1)$$

where $I_r(x,y,t)$ is the raw LIF image intensity, $\bar{I}_c(x,y,t)$ the calibration image intensity and $\bar{I}_{bg}(x,y,t)$ the background image intensity. The calibration image was taken with the flume filled with dyed water from the surface flow tank (tank 1), while the background image was taken with the flume filled with undyed water from the boundary layer flow tank (tank 0) at the start of the experiment. The overbars indicate averaging of 50 images. This leads to $I(x,y,t) = 0$ for water originally from the tank 0 and $I(x,y,t) = 1$ for water originally from tank 1. Figure 2 shows a processed LIF intensity image from experiment Set 3.

Figure 2: LIF image from Set 3.

We define a buoyancy variable θ as the buoyancy of a parcel of fluid measured relative to the density of the water originally in the boundary layer flow tank (tank 0), that is

$$\theta(x,y,t) = \frac{g(\rho_0 - \rho(x,y,t))}{\rho_0}. \qquad (2)$$

Here g is the acceleration due to gravity, $\rho(x,y,t)$ the density of the fluid parcel and ρ_0 the density of the water originally in tank 0. θ is determined from the normalized LIF intensity I as:

$$\theta(x,y,t) = I(x,y,t)\frac{g(\rho_0 - \rho_1)}{\rho_0}, \qquad (3)$$

where ρ_1 is the density of the water in the surface flow tank. While the density of the surface flow jets ρ_j is constant ($\rho_j = \rho_1$) for a given experiment, the bulk density of the boundary layer fluid ρ_b varies both along the length of the flume, due to dilution by the surface flow, and over time due to dilution of the water in tank 0, which is recirculated.

The actual buoyancy of a parcel is the buoyancy relative to its local environment, namely the local bulk flow buoyancy Θ_b. This is determined by integrating

$$u_b(x,t) = \frac{1}{\delta_b}\int_0^{\delta_b} u(x,y,t)dy, \qquad (4)$$

$$\theta_b(x,t) = \frac{1}{\delta_b U_b}\int_0^{\delta_b} \theta(x,y,t)u(x,y,t)dy, \qquad (5)$$

where $\theta(x,y,t)$ is obtained from the LIF, and the streamwise velocity $u(x,y,t)$ from the PIV, interpolated onto a common grid as described above. The average local bulk density Θ_b and bulk velocity U_b for each experimental run are determined by averaging $\theta_b(x,t)$ and $u_b(x,t)$ over the time of the run and across the measurement zone in the streamwise direction. The same ranges were also used to calculate all other statistics to be presented below. For the results presented in this paper we averaged over a period of 2 minutes (240 image pairs at 2 Hz) and a horizontal width of $\Delta x = 45$ mm. The change in Θ_b and U_b over 45 mm can be determined using the equations derived below and were $\delta\Theta_b/\Theta_b \approx \delta U_b/U_b \approx 0.1\%$. The change in buoyancy with time is estimated from the total surface flow rate (3.2 L/min) and the initial volume of tank 0 (800 L) giving a change of $\delta\Theta_b/\Theta_b \approx 0.8\%$ over a 2 minute averaging period.

Scaling

In this study we are comparing three experimental data sets with different surface conditions. To compare these data sets we derive a set of length, velocity and buoyancy scales, that include the extra mass, momentum and buoyancy fluxes resulting from the surface flows, so that we have scales that provide a consistent normalization across all three cases.

The effect on the boundary layer of the extra surface fluxes is determined by integrating the governing fluid flow equations vertically over the height of the channel. Integration of the mass conservation equation gives an equation for the streamwise divergence of the bulk velocity,

$$\delta_b \frac{dU_b}{dx} = V_s. \qquad (6)$$

Here V_s is the mean surface flux velocity which is related the surface jet velocity through $V_s = A_r v_j$. Integration of the streamwise momentum equation gives the effect of the additional momentum flux on the streamwise force balance within the boundary layer:

$$\frac{\delta_b}{\rho_b}\frac{dP_b}{dx} = -\delta_b U_b \frac{dU_b}{dx} - \nu \frac{\partial U}{\partial y}_{y=0}, \qquad (7)$$

Set	Re_b	Re^*_τ	Ri	δ_b	U_b	U_∞	v_j	V_s	Θ_b	Θ_∞	θ_j	Θ_s	$\Delta\Theta$	u^*_τ	θ^*_τ	$u^*_\tau\theta^*_\tau$
1	6320	365	0	35.1	162	187	0	0	0	0	0	0	0	9.35	0	0
2	6440	365	0	37.9	153	179	0.677	0.142	0	0	0	0	0	8.66	0	0
3	6840	486	-0.127	43.5	142	152	0.677	0.142	37.2	35.2	490	103	67.8	10.1	6.41	64.5

Table 1: Experimental parameters. Dimensions used are: lengths (mm), velocities (mm/s) and buoyancy (mm/s^2).

where U is the mean velocity at height y, ν the kinematic viscosity, and P_b the pressure. Combining (6) and (7) gives

$$\frac{\delta_b}{\rho_b}\frac{dP_b}{dx} = -U_b V_s - \nu \frac{\partial U}{\partial y}_{|y=0}. \tag{8}$$

Based on this we define a modified wall unit velocity and length scales as:

$$u^*_\tau = \sqrt{U_b V_s + \nu \frac{\partial U}{\partial y}_{y=0}}, \qquad \delta^*_\tau = \frac{\nu}{u^*_\tau}. \tag{9}$$

For the buoyant case, integration of the transport equation for the buoyancy variable θ gives,

$$V_s(\theta_j - \Theta_b) = \delta_b U_b \frac{d\Theta_b}{dx}, \tag{10}$$

where θ_j is the buoyancy in the surface flow jets. Thus the appropriate scale for the surface buoyancy flux is,

$$\theta^*_\tau = \frac{V_s(\theta_j - \Theta_b)}{u^*_\tau}. \tag{11}$$

Results and Discussion

The flow parameters for the results presented are shown in Table 1. Here $Re^*_\tau = u^*_\tau \delta_b/\nu$ is the Reynolds number based on the the modified surface shear velocity scale u^*_τ. The bulk Richardson number $Ri = \Delta\Theta\delta_b/U^2_\infty$ is formulated in terms of the upper free surface velocity U_∞ and mean buoyancy difference $\Delta\Theta = \Theta_s - \Theta_\infty$ across the boundary layer. Here the mean buoyancy at the surface, Θ_s, is calculated as the product of the open/closed area ratio of the surface, A_r, and the buoyancy of the jets, that is, $\Theta_s = A_r\theta_j$. The surface buoyancy flux is $u^*_\tau\theta^*_\tau$.

Results are presented in the Figures 3–6. In these figures a superscript $*$ indicates non-dimensionalization using the surface flux scales described above. For Sets 1 and 2 the modified surface friction velocity u^*_τ was determined from the mean velocity at the lowest data point, which was within the laminar sublayer ($y^* < 5$) in both cases. For Set 3, the PIV data at the first point ($y = 0.45$ mm) appeared to contain large errors and was not considered reliable. In this case u^*_τ was detemined by estimating $U(y^* = 5)$ using cubic Hermite extrapolation from the overlying data points. The scaled mean buoyancy Θ^* is measured relative to the mean buoyancy at the surface, that is $\Theta^*(y^*) = (\Theta(y^*) - \Theta_s)/\theta^*_\tau$.

The mean velocity profile for Set 1 in Figure 3 is in excellent agreement with the theoretical log law line, showing that we are accurately measuring mean velocity down to the laminar sublayer, and that our meshed surface is acting as a smooth surface. The profile for Set 2 with neutral surface flow overlays Set 1 up to $y^* \approx 100$. This indicates that the modified surface flux velocity scaling presented above is successfully accounting for the effect of additional mass and momentum fluxes at the surface. When the mean velocity profile is plotted in terms of standard wall units (not shown), the profiles do not overlay. There is a small divergence of the two profiles in the wake region at the top of the channel, which we believe to be due to divergence of the velocity field in Set 2 as a result of the surface mass flux upstream of the measurement zone. The velocity profile for Set 3, with a buoyant surface flow, shows the expected steepening of the boundary layer due the enhanced mixing driven by the buoyant convective plumes.

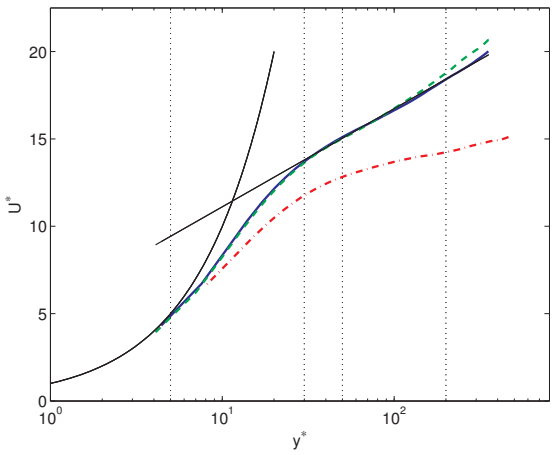

Figure 3: Mean velocity profile. Blue solid line–Set 1 (no surface flow). Green dashed line–Set 2 (non-buoyant surface flow). Red dash-dot line–Set 3 (buoyant surface flow). Solid black lines are $U^* = y^*$ and $U^* = \frac{1}{\kappa}\ln y^* + 5.5$ with $\kappa = 0.41$.

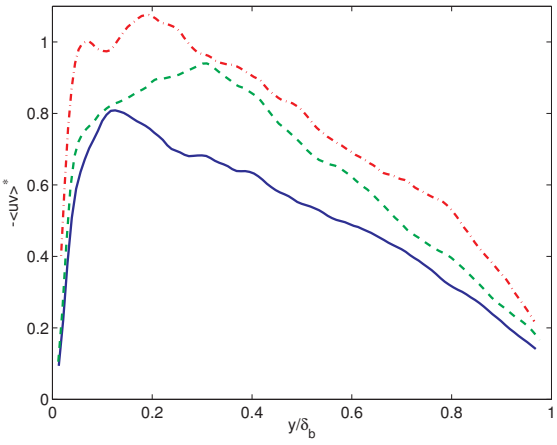

Figure 4: Turbulent shear stress. Key as in Figure 3.

Figure 4 compares profiles of turbulent shear stress. The shear stress profile for the non-convecting case (Set 1) shows the expected linear profile down to $y/\delta_b = 0.1$. The profile for Set 2 shows a significant enhancement of the shear stress, with the profile peaking at $y/\delta_b \approx 0.3$. It appears that the interaction between the vertical surface jets and the horizontal boundary layer flow leads to additional shear production of turbulence in the

near-wall region. We can however compare Sets 2 and 3, which have the same surface jet velocities. The profiles for Sets 2 and 3 are similar down to $y/\delta_b = 0.3$. Below this height, the buoyant case has a region of relatively constant stress $-\langle uv \rangle^* \approx 1$, ie. equal to the effective wall shear stress. This is similar to the constant flux region seen in the near wall region of thermally convecting boundary layers such as the surface layer of the atmospheric boundary layer.

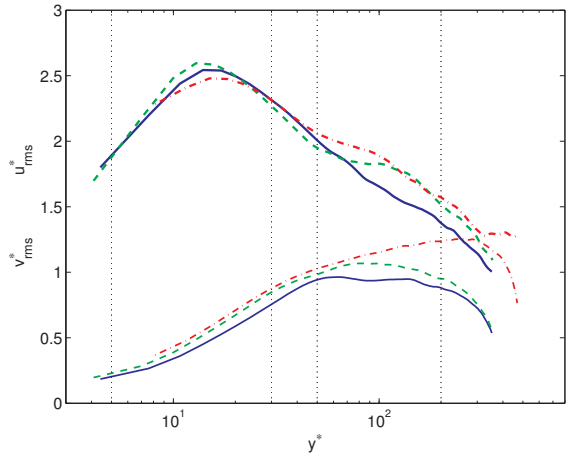

Figure 5: Streamwise and vertical velocity fluctuations. Key as in Figure 3.

Figure 5 compares profiles of streamwise and vertical velocity fluctuations. The profiles for for Sets 1 and 2 are in good agreement with those measured in other experiments and in Direct Numerical Simulations (DNS) of neutral channel flow at similar Re_τ (see for example [2]). The measured values in our experiment are $5-10\%$ lower than the DNS results. For Set 2, both streamwise and vertical fluctuations are slightly higher than for Set 1 across most of the boundary layer, presumably due to the extra shear production associated with the surface jets discussed above. For the buoyant convection case, the streamwise fluctuations are quite similar to those for the neutral cases, however, there is a substantial increase in the vertical velocity fluctuations above $y^* = 100$ due to buoyancy production of turbulence kinetic energy. This behaviour is typical of convective boundary layers, where shear production of turbulence dominates in the near wall region, while buoyancy production dominates in the outer region. There also appears to be a small dampening of the streamwise fluctuations in the near wall region in the buoyant flow.

Figure 6 shows the mean velocity and buoyancy profiles for Set 3. The buoyancy profile was measured down to a height of $y = 0.1$ mm or $y^* \approx 1$ which is well within the laminar sublayer. This profile shows some noteworthy features. Θ^* is tending towards zero implying that the unscaled measured value Θ derived from the LIF is tending towards the Θ_s. Since Θ_s is defined in terms of measurements independent of the LIF measurements (see above) this is a strong indication that our LIF method is giving accurate results. The gradient $d\Theta^*/dy^*$ is also tending towards zero as the wall is approached within the laminar sublayer. This is consistent with the fact that we have a advective flux-type boundary condition for buoyancy at the surface – a conserved scalar introduced within a boundary mass flux. Interestingly, the Θ^* profile shows a distinct logarithmic region in the range $7 < y^* < 25$, which corresponds to the non-logarithmic buffer zone in the velocity boundary layer.

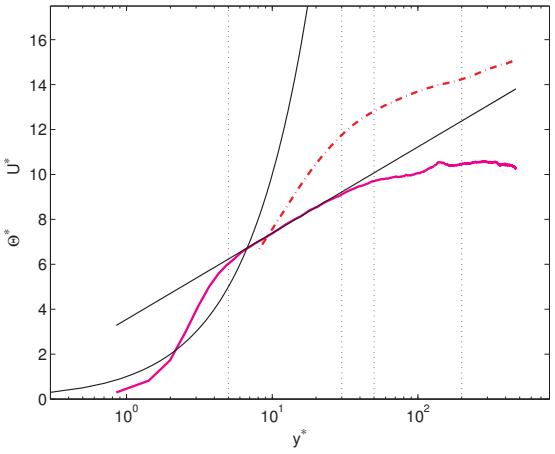

Figure 6: Mean velocity and buoyancy profiles for Set 3. Red dash-dot–mean velocity. Solid magenta–mean buoyancy.

Conclusions

Results have been presented for turbulent open channel flow over a flat porous plate with three different surface conditions.

The results give an indication of the accuracy of our experimental approach. The accuracy of our LIF method is demonstrated in particular by the accurate measurement of the buoyancy field within the laminar sublayer. The mean velocity measurements obtained with the PIV for the no-surface-flow case are in excellent agreement with the log law, while turbulent stress and fluctuation profiles are in good agreement with other published results.

A scaling has been derived that accounts for the effect of the mean mass, momentum and buoyancy fluxes through the surface. This scaling gave scaled mean velocity profiles that overlay one another in the buffer zone and log law region for the no-surface-flow and neutral-surface-flow cases. The surface jets were found to give an increase in turbulent fluctuations and shear stress. We suggest that this is due to the interaction between the jets and the horizontal boundary layer flow providing an extra source of shear production in the near wall region.

The buoyant-surface-flow case shows promising similarities with thermal convecting boundary layers, including a constant stress region in the surface layer and enhanced vertical fluctuations due to buoyancy production in the outer region. A logarithmic region in the mean buoyancy profile has also been identified, located in the buffer zone. These features are the subject of ongoing investigation.

Acknowledgements

This work has been supported by an Australian Research Council Discovery Project Grant DP110102343.

References

[1] Kirkpatrick, M. P., Starner, S. H., Williamson, N. and Armfield, S. W., A new experimental rig for investigations of sheared convective boundary layers, in *Proc. 18th AFMC*, Launceston, TAS, 2012.

[2] Moser, R. D., Kim, J. and Mansour, N. N., Direct numerical simulation of turbulent channel flow up to Re = 590, *Phys. Fluids*, **11**, 1999, 943945.